ОБЪЕДИНЕННЫЙ
ИНСТИТУТ
ЯДЕРНЫХ
ИССЛЕДОВАНИЙ

Дубна

E6-96-454

I.N.Izosimov[1], V.G.Kalinnikov, M.Yu.Myakushin[1],
A.A.Rimski-Korsakov[1], A.A.Solnyshkin, J.Suhonen[2],
J.Toivanen[2]

STRUCTURE OF THE β^+ (EC) DECAY STRENGTH FUNCTION OF ^{147g}Tb ($T_{1/2} \simeq 1.6$ h)

Submitted to «Nuclear Physics A»

[1]V.G.Khlopin Radium Institute, 194021, St.Petersburg, Russia
[2]Department of Physics, University of Jyväskylä, P.O.Box 35,
FIN-40351 Jyväskylä, Finland

1996

1. Introduction

The β decay strength function $S_\beta(E)$ is one of the most important characteristics of the atomic nucleus. It reflects the distribution of the squared β-decay matrix elements with respect to the excitation energy of the nuclear states of the daughter nucleus [1]. For beta transitions of the Gamow–Teller type $S_\beta(E)$ can be written down as [2]:

$$S_\beta(E) = \frac{B'_\mp(\mathrm{GT}, E)}{D(g_V^2/g_A^2)}, \tag{1}$$

$$B'_\mp(\mathrm{GT}, E) = \frac{4\pi}{g_A^2} B_\mp(\mathrm{GT}, E) = \frac{1}{2I_i + 1} |\langle I_f \| \sum_{k,\mu} t_\mp(k)\sigma_\mu(k) \| I_i \rangle|^2, \tag{2}$$

where I_i and I_f are the spins of the initial and final states, g_A and g_V are the constants of the axial-vector and vector components of the β decay, $D = (6260 \pm 60)$ s, and $t_\mp\sigma$ is the product of the isospin and spin operators giving the respective operators of the Gamow–Teller β^- or β^+(EC) decays.

Level occupancy after the β decay, $I(E)$, and the half-life, $T_{1/2}$, are related to $S_\beta(E)$ by the equations [2]:

$$I(E) = S_\beta(E) T_{1/2} f(Q_\beta - E), \tag{3}$$

$$T_{1/2}^{-1} = \int_0^{Q_\beta} S_\beta(E) f(Q_\beta - E) dE, \tag{4}$$

where Q_β is the total energy available for the β decay and $f(Q_\beta - E)$ is the Fermi function [3].

The structure of $S_\beta(E)$ depends on the structure of the atomic nucleus and on the isovector component of the effective nucleon-nucleon interaction. Information on the structure of $S_\beta(E)$ is important for different fields of nuclear physics. Prediction of nuclear half-lives [4], analysis of delayed processes [5], analysis of element yields in astrophysical processes [6], in thermonuclear processes [7], in cosmochronology [8], and in technological

calculations [5,8] require knowledge of the structure of strength functions for β-transitions.

The present paper deals with the experimental and theoretical study of the structure of the strength function for the β^+(EC) decay of the ^{147g}Tb nucleus. This nuclide is chosen because it is near the doubly magic nucleus ^{146}Gd and thus it is a suitable object for testing different theoretical approaches [9]. Besides, its total β^+(EC) decay energy is quite high ($Q_{EC} \simeq 4.6$MeV) and it can be produced in the Z-separated (radiochemically) and A-separated (by mass separation) forms.

2. Experimental techniques and data processing

2.1. Production of sources

The ^{147g}Tb (1.6 h) source was produced in the spallation reaction with tantalum exposed to the internal 660-MeV proton beam from the LNP JINR Phasotron . Half an hour after the exposure the tantalum target was dissolved and the Tb fraction was separated by chromatographic techniques. The ^{147}Tb nuclides were isolated by mass separation of the terbium fraction at the YASNAPP-2 mass separator [10]. The ^{147}Tb ions were collected on an Al foil and investigated with a total absorption gamma ray spectrometer (Fig. 1).

2.2. Gamma ray total absorption spectrometer

The total absorption spectrometer [11] of gamma rays consists of the NaI(Tl) crystals 200 mm by 110 mm and 200 mm by 140 mm in size. The larger crystal has a 70 mm by 80 mm well into which the nuclei under investigation are supplied (Fig. 1) and where a Si(Au) detector is installed. Its sensitive layer is 2 mm thick, and it allows detecting beta particles.

Operation of the total absorption spectrometer (TAS) is based on summation of cascade gamma quantum energies in the 4π geometry. With the photopeak efficiency of TAS exponentially depending on the energy, the area of the total absorption peak in discharge of a level by a cascade of gamma quanta does not depend on the decay scheme, and the detection efficiency in the total absorption peak is equal to the photopeak detection efficiency for a gamma quantum with an energy equal to the energy of

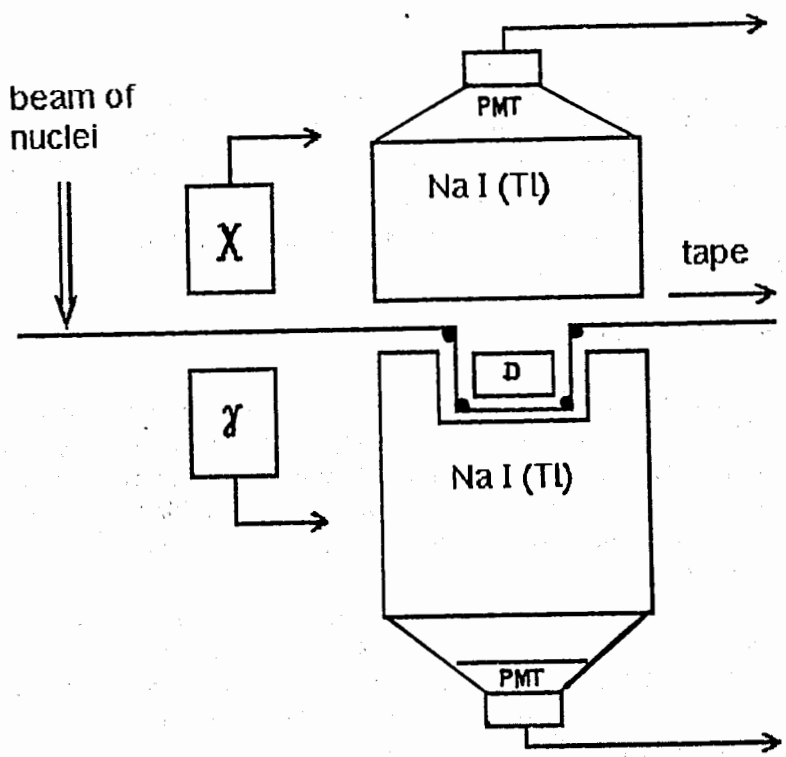

Figure 1: Experimental lay-out for measurement of TAS-gamma-spectra. After mass separation the nuclei to be studied are transported either to the Ge(Li) detector and HP X-ray detector or to the well of the 4π NaI(Tl) detector. In the well of the NaI(Tl) crystall there is a Si(Au) detector (D) of beta particles, wich allows TAS-gamma-spectra to be measured in coincidence with beta particles. PMT–photomultipliers.

the populated level [2]. Using sources with the known absolute efficiency, we experimentally found the total absorption efficiency ϵ_{tot} of a gamma quantum cascade to be in the range 0.6–4.2 MeV. In this range ϵ_{tot} exponentially depends on the total gamma quantum cascade energy E with an error below 6%:

$$\epsilon_{tot} = \exp(-0.44E). \tag{5}$$

Relation (5) does not hold at $E_\gamma > 5$ MeV. Analyzing spectra from TAS at $E > 5$ MeV, one must take special measures. In the present paper we investigated the structure of $S_\beta(E)$ at $E \leq 4.2$ MeV, where (5) is valid.

Isolating total absorption peaks in the TAS spectrum, one can find the occupancy of the levels $I(E)$, and using (2), find the strength function $S_\beta(E)$. The end-point energy of TAS spectra is related to the total electron-capture energy Q_{EC} [2].

2.3. Electronics

Scintillation in the NaI(Tl) crystals is recorded by two photomultipliers FEU-173-1. The crystals are connected to the photomultipliers by a hollow light guide with a dull inner surface. Signals from the photomultipliers and from the semiconductor Si(Au) detector are amplified and sent to the analog-to digital converters (ADC) PA-24K, whose inputs are normally disabled (Fig. 2).

At the same time signals pass through fast amplifiers and arrive at the constant fraction (CF) shapers. The thus conditioned semiconductor detector signal triggers the controlling unit KL-23K. This unit shapes a signal of certain duration applied to bus R2 of the CAMAC highway, which enables inputs of all ADCs. Thus, the logic of fast $\beta - \gamma$ coincidences is realized. Also, a "start" signal is picked off from the front panel of KL-23K to trigger the multistop time-to-digital converter (TDC). The "stop" signals for the TDC are delayed time signals from the CF shapers in both gamma channels. The information on the time of signals appearance in the γ-channel with respect to appearance of signals in the β-channel is used for subsequent event selection. The set-up and data taking are controlled by a personal computer connected to the CAMAC highway through a crate controller KK-009.

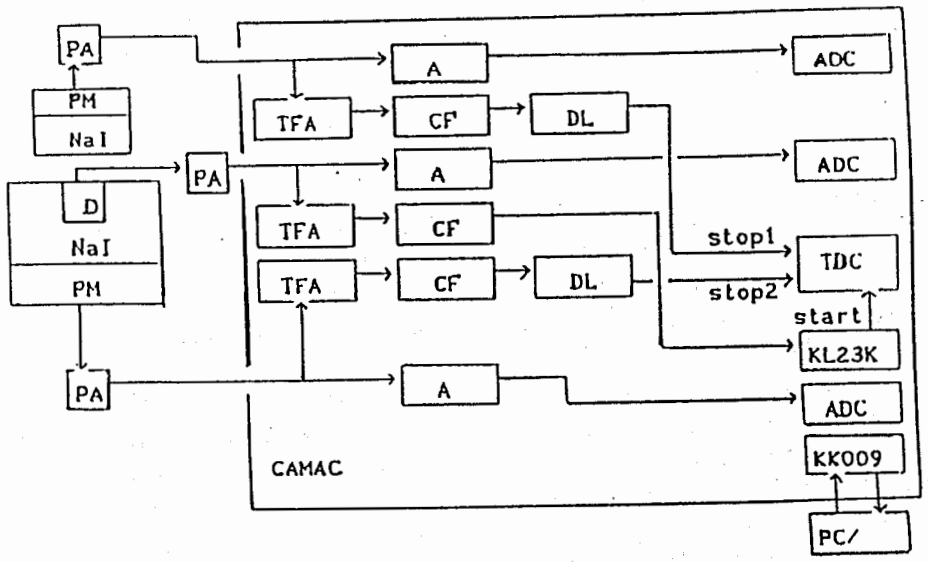

Figure 2: Schematic view of the total absorption spectrometer (TAS). The 4π NaI(Tl) gamma detector is shown on the left. PM–photomultipliers, D—Si(Au) detector of beta particles, PA–preamplifiers, A–amplifiers, TFA–fast amplifiers, CF–shapers, DL–delay lines, ADC–analog-to-digital convertor, TDC–time-to-digital convertor, KL23K–control unit, KK009–crate controller.

2.4. Data processing

The following corrections were taken into account in the processing of the experimental data.

1. In the energy region near Q_{EC} there can be distortions due to accidental summation of gamma quanta from decay of different nuclei by NaI(Tl) crystals (pile-up spectrum). We considered the pile-up spectrum under the assumption that the amplitude of the total signal A_{1+2} is equal to the sum of the amplitudes of signals A_1 and A_2. In this case, for the pile-up spectrum we can use the expression [12]:

$$S_p(n) = \text{const} \sum_{j=1}^{n} S(j)S(n-j), \quad n = 1, 2, 3, ..., K, \tag{6}$$

where $S_p(n)$ is the number of pile-ups in channel "n", $S(j)$ is the counting in the $j-$th channel of the experimental spectrum and K is the maximum channel of the spectrum. The high-energy region of the spectrum near Q_{EC} was used for normalization (determination of "const" in eq. (4)).

Actually, the amplitude A_{1+2} depends on the time between the nuclear decays and varies from A_1, A_2 to $A_1 + A_2$, which results in a spread-out shape of the pile-up spectrum in the low-energy region (where pile-ups are less than 1% of the experimental spectrum) while in the high-energy region (near Q_{EC}) the shape o the pile-up spectrum practically does not change. The absolute value of the pile-up spectrum may change in the high-energy region, which is corrected by calculating normalization in (6) by experimental points. Normalization in (4) is calculated as follows:

$$\text{const} = \frac{\sum_{n=n_1}^{K} (S(n) - S_f(n))}{\sum_{n=n_1}^{K} \sum_{j=1}^{n} S(j)S(n-j)}, \tag{7}$$

where $S_f(n)$ is the background in the $n-$th channel. In our experiments the total pile-up intensity did not exceed 9% of the total background intensity.

2. The correction for the dead time of the measuring system was found by measuring the count of the stable frequency and amplitude generator.

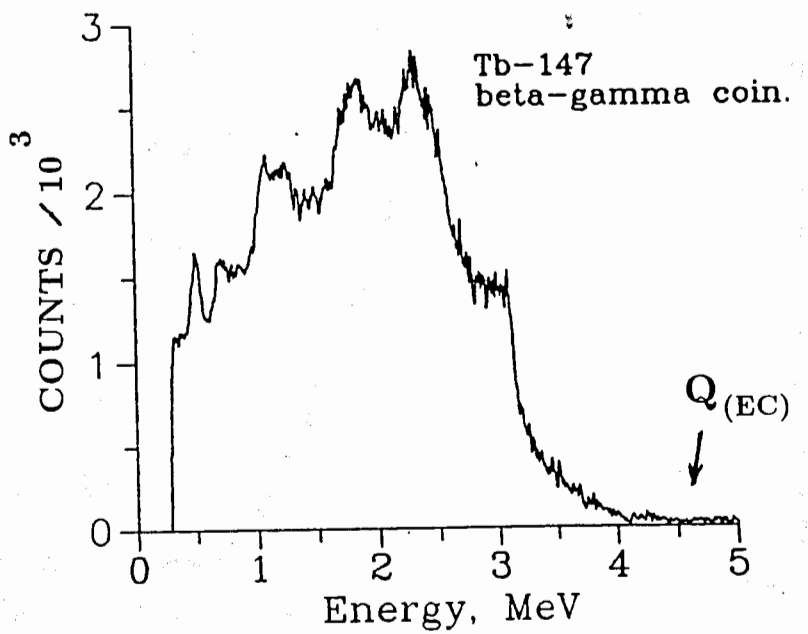

Figure 3: Gamma ray spectrum measured with a total absorption spectrometer (TAS-gamma-spectrum) in coincidence with β^+ particles from the β^+ decay of ^{147g}Tb.

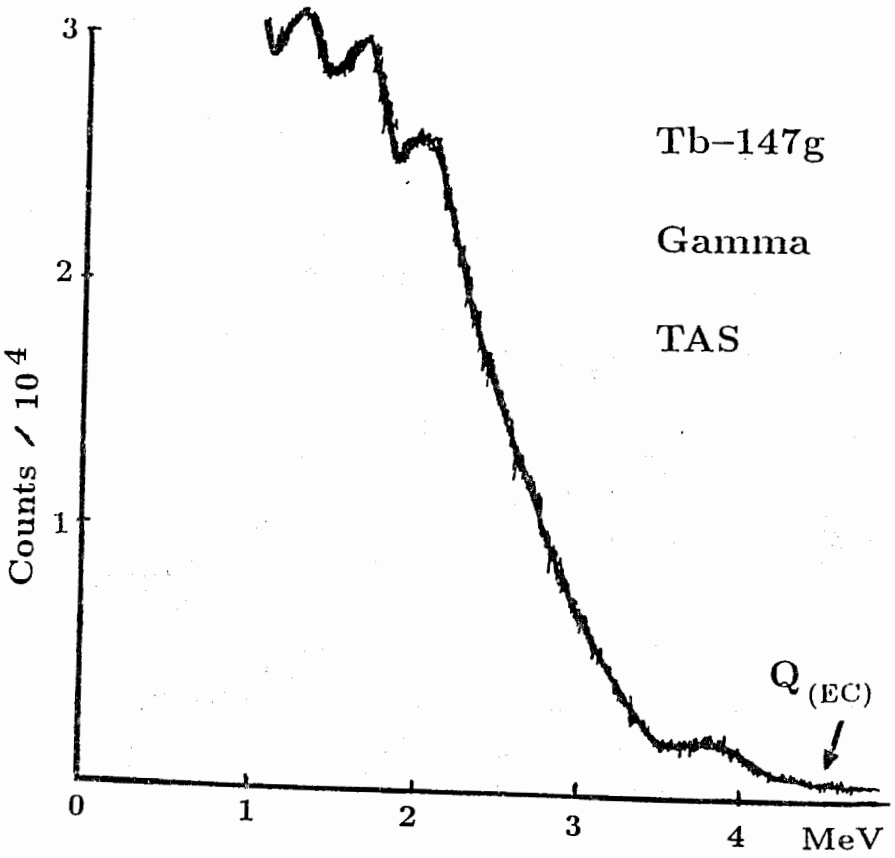

Figure 4: Gamma ray spectrum from the $\beta^+(EC)$ decay of ^{147g}Tb measured with a total absorption spectrometer (TAS-gamma-spectrum) without coincidence with β particles.

3. The background was measured in intervals between source measurements. The background varied but slightly in the course of measurement and its consideration virtually does not introduce an additional error.

The main task in processing of TAS spectra at $E \leq 5$ MeV is to reveal total absorption peaks. For them, $S_\beta(E)$ is determined quite reliably because the area of the total absorption peak at $E < 5$ MeV does not depend on the level de-excitation scheme [2]. But it is rather difficult to interpret the rest of the spectrum because the shape of the continuous distribution and intensity of the incomplete summation peaks depend on the decay scheme. With few (≤ 3) peaks remaining in the spectrum (after revealing total absorption peaks) and the known TAS response function, it is possible to analyze all peaks in the spectrum [2, 13].

Figure 3 displays a TAS spectrum of gamma rays measured in coincidence with β^+ particles in the β^+(EC) decay of ^{147g}Tb. The time resolution of the spectrometer was about 2 μs. Figure 4 shows a TAS spectrum of gamma rays measured in the decay of ^{147g}Tb but without coincidence with β^+ particles.

The peaks of maximum energy ($E \simeq 4$ MeV in Fig. 4 and $E \simeq 3$ MeV in Fig. 3) are total absorption peaks.

3. Strength function for β^+(EC) decay of ^{147g}Tb

Using the procedure of analysis of total absorption spectrum described in [2] and our TAS-gamma-spectra, we constructed a strength function for the β^+(EC) decay of ^{147g}Tb (Fig. 5a).

Peaks in $S_{\beta^+(EC)}$ at excitation energies of the ^{147}Gd nucleus $E \simeq 4$ MeV and $E \simeq 2$ MeV are related to the total absorption peaks in the TAS-gamma-spectra and are obtained directly from the analysis of the experimental data without any assumptions of the decay scheme. The peak in $S_{\beta^+(EC)}(E)$ at $E \simeq 1.5$ MeV is obtained under the model assumption that gamma de-excitation of levels populated by the β^+(EC) decay involves two gamma quanta of equal energy. Thus, the peak in $S_{(EC)}(E)$ (Fig. 5a) at $E \simeq 4$ MeV and peak in $S_{\beta^+(EC)}$ at $E \simeq 2$ MeV are established quite reliably while the peak at $E \simeq 1.4$ MeV requires further investigation.

Detailed study of the decay and population scheme of low-spin states in ^{147}Gd during the β^+(EC) decay of ^{147g}Tb was carried out in [9] with Ge(Li)

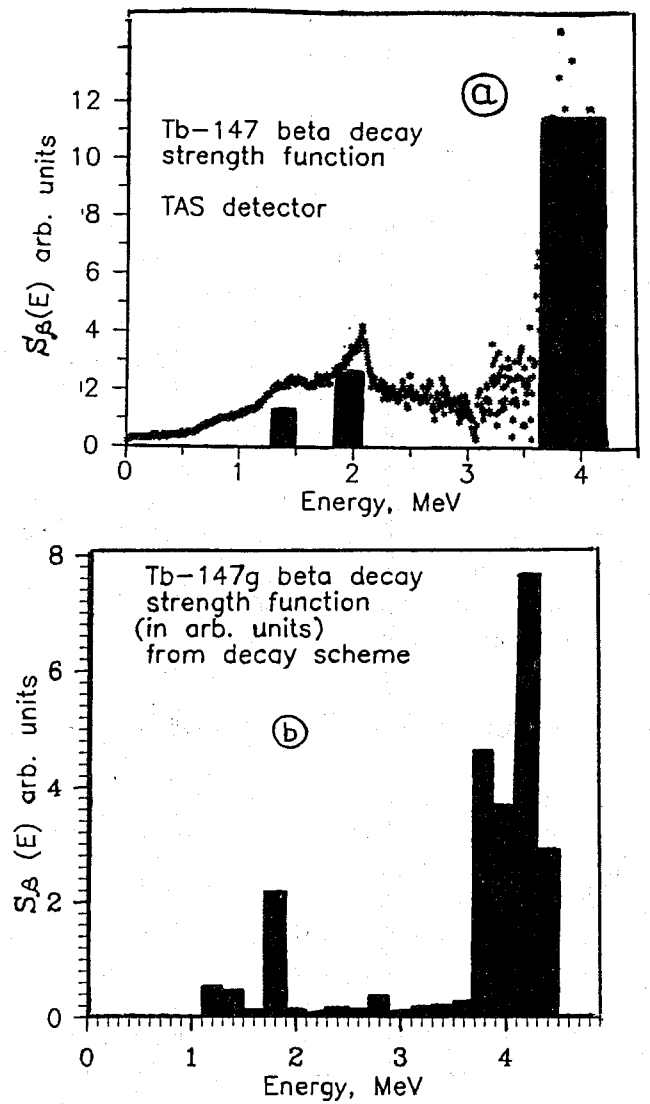

Figure 5: a). Strength function for $\beta^+(EC)$ decay of ^{147g}Tb (relative units) dedused from the analysis of TAS-gamma-spectra. b). Strength function for the $\beta^+(EC)$ decay of ^{147g}Tb (relative units) deduced from the analysis of the ^{147g}Tb decay scheme from [9].

and HP Ge detectors. Using the data from [9], we constructed $S_{\beta^+(\mathrm{EC})}(E)$ for β^+(EC) decay of ^{147g}Tb (Fig. 5b). The energies and relative intensities of peaks at $E \simeq 4$ MeV and $E \simeq 2$ MeV agree well for $S_{\beta^+(\mathrm{EC})}(E)$ derived from the analysis of the TAS-gamma-spectra (Fig. 5a) and for $S_{\beta^+(\mathrm{EC})}(E)$ derived from the analysis of ^{147g}Tb decay scheme (Fig. 5b). The intensity of the peak at $E \simeq 1.5$ MeV in $S_{\beta^+(\mathrm{EC})}(E)$ derived from the analysis of the TAS-gamma-spectra exceeds the intensity of the peak in $S_{\beta^+(\mathrm{EC})}(E)$ derived from the analysis of the ^{147g}Tb decay scheme. This difference stems from the model assumptions used by us in the analysis of the TAS-gamma-spectra in excitation energy region $E \simeq 1.5$ MeV. Good agreement of $S_{(\mathrm{EC})}(E)$ and $S_{\beta^+(\mathrm{EC})}(E)$ peak energies and intensities at $E \simeq 4$ MeV and $E \simeq 2$ MeV indicates good agreement with the ^{147g}Tb decay scheme proposed in [9] and/or validity of the $S_{\beta^+(\mathrm{EC})}(E)$ determination from TAS-gamma-spectra provided that total absorption peaks are identified.

4. Theoretical framework

4.1 Energies and wave functions of the odd nucleus

We start our nuclear-structure calculation from a realistic hamiltonian containing a diagonal one-body part (the mean-field single-particle part) and a two-body residual interaction part containing antisymmetrized two-body matrix elements obtained by G-matrix methods from the Bonn one-meson-exchange potential [14]. Defining the particle creation and annihilation operators, $c^\dagger$ and c, we obtain

$$H = \sum_{\alpha} \varepsilon_\alpha c^\dagger_\alpha c_\alpha + \frac{1}{4} \sum_{\alpha\beta\gamma\delta} \bar{v}_{\alpha\beta\gamma\delta} c^\dagger_\alpha c^\dagger_\beta c_\delta c_\gamma \,, \tag{8}$$

where we have used the convention that in the creation and annihilation operators greek indices denote all single-particle quantum numbers $\alpha = \{a, m_a\}$, and roman indices, when used, denote all single-particle quantum numbers except the magnetic ones, i.e. $a = \{n_a, l_a, j_a\}$. The antisymmetrised two-body interaction matrix element is defined as $\bar{v}_{\alpha\beta\gamma\delta} = \langle\alpha\beta|v|\gamma\delta\rangle - \langle\alpha\beta|v|\delta\gamma\rangle$. The approximate ground state of the even-even reference nucleus is obtained from a BCS calculation, where quasiparticle energies and occupation factors u_a and v_a are obtained by making a Bogoliubov transformation to quasiparticles

$$
\begin{aligned}
a^{\dagger}_{\mu} &= u_{\mu} c^{\dagger}_{\mu} - v_{\mu} \tilde{c}_{\mu} \\
\tilde{a}^{\dagger}_{\mu} &= u_{\mu} \tilde{c}^{\dagger}_{\mu} + v_{\mu} c_{\mu} \,,
\end{aligned} \tag{9}
$$

where $\tilde{a}^{\dagger}_{\mu} = a^{\dagger}_{-\mu}(-1)^{j+m}$ and $\tilde{c}^{\dagger}_{\mu} = c^{\dagger}_{-\mu}(-1)^{j+m}$. After this transformation the hamiltonian can be written in the form:

$$
H = \sum_{\alpha} E_{a} a^{\dagger}_{\alpha} a_{\alpha} + H_{22} + H_{40} + H_{04} + H_{31} + H_{13} \,, \tag{10}
$$

where E_a are the quasiparticle energies and other terms of the hamiltonian are normal-ordered parts of the residual interaction labeled according to the number of quasiparticle creation and annihilation operators which they contain [15].

The optimal quasiparticle energies and occupation factors are obtained by comparing the results of a BCS calculation with the data for the even-even nuclei involved in the calculation. The monopole matrix elements of the two-body interaction are scaled by the pairing-strength parameters (separately for protons and neutrons) whose value can be determined by comparison with the semiempirical pairing gaps obtained from the proton and neutron separation energies [15].

In our method of calculation we use in eq. (8) the Coulomb-corrected Woods–Saxon single-particle energies ε_{α} with the parametrization of [16]. By performing the BCS calculation in this basis and comparing the resulting quasiparticle spectrum with the low-energy spectrum of the neighboring proton-odd and neutron-odd nuclei we obtain information about the validity of the Woods–Saxon parametrization of the mean field. If necessary, the proton or neutron single-particle energies can be adjusted in the vicinity of the fermi surface in order to achieve a more realistic description of the one-quasiparticle properties of the neighboring odd nuclei.

In the next step a correlated ground state and the excited states of the even-even reference nucleus are constructed by using the quasiparticle random-phase approximation (QRPA). In the QRPA the creation operator for an excited state (QRPA phonon) has the form:

$$
Q^{\dagger}_{\omega} = \sum_{a \le a'} \left(X^{\omega}_{aa'} A^{\dagger}(aa'; J_{\omega} M) - Y^{\omega}_{aa'} \tilde{A}(aa'; J_{\omega} M) \right) \,, \tag{11}
$$

where the quasiparticle pair creation and annihilation operators are defined in the following way $A^{\dagger}(aa'; JM) = \sigma^{-1}_{aa'} \left[a^{\dagger}_{a} a^{\dagger}_{a'} \right]_{JM}$, $\tilde{A}(aa'; JM) = \sigma^{-1}_{aa'} \left[\tilde{a}_{a} \tilde{a}_{a'} \right]_{JM}$ and $\sigma_{aa'} = \sqrt{1 + \delta_{aa'}}$. The greek indices in the context of a phonon creation or annihilation operator denote phonon spin J and parity π. Furthermore, they contain an additional quantum number k enumerating the different QRPA roots for the same angular momentum and parity. Thus $\omega = \{J_{\omega}, \pi_{\omega}, k_{\omega}\}$. For each value of the angular momentum and parity the spectrum of the even-even nucleus is constructed by diagonalizing the QRPA matrix containing the usual submatrices A (quasiparticle-quasiparticle interaction) and B (induced by correlations of the ground state) [17]. The two-body matrix elements of multipolarity J^{π}, occurring in the A and B matrices, are multiplied by two phenomenological scaling constants, namely the particle-hole strength, $g_{\rm ph}$, and the particle-particle strength $g_{\rm pp}$ [18]. In the present calculation the bare G-matrix value of $g_{\rm pp} = 1.0$ has been used for all multipolarities. The value of $g_{\rm ph}$ can be set by the experimental value of the energy of the first J^{π} state and/or the electromagnetic decay rate of the J^{π} state to the ground state.

It has to be pointed out that the even-even reference nucleus has been used to scale the monopole-pairing part of the two-body matrix elements in the BCS calculation and to scale the particle-hole and particle-particle channels of the other multipolarities in the QRPA calculation. This scaling has fixed the $|T_z| = 1$ interaction part of the hamiltonian (8) and only the proton-neutron interaction part is still free for adjustment. However, in this work we have not scaled the proton-neutron interaction part (the $H_{31} + H_{13}$ part of the quasiparticle hamiltonian in eq. (10)) but, instead, used the bare G matrix to describe qualitatively the strength function of the β^{+}(EC) decay of ^{147}Tb. In this case even a qualitative agreement with experiment would yield the needed interpretation of the experimental results.

The basis states in our quasiparticle-phonon calculation are constructed from the previously determined BCS quasiparticles and the QRPA phonons of the studied even-even reference nucleus. Our microscopic quasiparticle-phonon model (MQPM) makes the following ansatz for states in an even-

odd nucleus

$$|i;jm\rangle = \left(\sum_n C^i_n a^\dagger_{njm} + \sum_{nj'\alpha} C^i_{nj'\alpha} \left[a^\dagger_{nj'} Q^\dagger_\alpha \right]_{jm} \right) |-\rangle \,, \tag{12}$$

where $|-\rangle$ denotes the QRPA vacuum of the even-even reference nucleus. The hamiltonian and overlap matrix elements between the quasiparticle - phonon states have the following quite simple form:

$$\langle -| \left[a_n Q_\alpha \right]^\dagger_j \left[a^\dagger_{n'} Q^\dagger_{\alpha'} \right]_j |-\rangle = \delta_{\alpha\alpha'}\delta_{nn'} + A\,(\alpha n \alpha' n'; j) \,, \tag{13}$$

$$\langle -| \left[a_n Q_\alpha \right]^\dagger_j H \left[a^\dagger_{n'} Q^\dagger_{\alpha'} \right]_j |-\rangle =$$

$$\tfrac{1}{2}\left(\hbar\Omega_\alpha + E_n + \hbar\Omega_{\alpha'} + E_{n'}\right) \langle -| \left[a_n Q_\alpha \right]^\dagger_j \left[a^\dagger_{n'} Q^\dagger_{\alpha'} \right]_j |-\rangle$$

$$+ \tfrac{1}{2} \hat{J}_\alpha \hat{J}_{\alpha'} \sum_a \left\{ \begin{array}{ccc} j_{n'} & j_a & J_\alpha \\ j_n & j & J_{\alpha'} \end{array} \right\}$$

$$\times \left(\hbar\Omega_\alpha - E_n + \hbar\Omega_{\alpha'} - E_{n'} + 2E_a\right) \bar{X}^\alpha_{an'} \bar{X}^{\alpha'}_{an} \sigma^{-1}_{an} \sigma^{-1}_{an'} \,,$$

where Ω_α denote the QRPA-phonon energies, and

$$A\,(\alpha n \alpha' n'; j) =$$

$$\hat{J}_\alpha \hat{J}_{\alpha'} \sum_a \left[\left\{ \begin{array}{ccc} j_{n'} & j_a & J_\alpha \\ j_n & j & J_{\alpha'} \end{array} \right\} \bar{X}^\alpha_{an'} \bar{X}^{\alpha'}_{an} - \frac{\delta_{jj_a}}{\hat{j}^2} \bar{Y}^\alpha_{an} \bar{Y}^{\alpha'}_{an'} \right] \sigma^{-1}_{an} \sigma^{-1}_{an'} \,. \tag{14}$$

Here $\sigma_{aa'} = \sqrt{1+\delta_{aa'}}$ and $\bar{X}^\alpha_{aa'} \equiv X^\alpha_{aa'} - (-1)^{j_a + j_{a'} - J_\alpha} X^\alpha_{a'a}$. The same definition holds for $\bar{Y}$. The interaction matrix elements between the one-quasiparticle and quasiparticle-phonon states have the following form:

$$\langle -| \left[Q_\alpha a_n \right]_{jm} \hat{H} a^\dagger_{\nu'} |-\rangle =$$

$$\tfrac{1}{3} \frac{\hat{J}_\alpha}{\hat{j}_{n'}} \sum_{a \le a'} H_{\rm pp}(nn'aa'J_\alpha) \left(u_a u_{a'} X^\alpha_{aa'} - v_a v_{a'} Y^\alpha_{aa'} \right) \sigma^{-1}_{aa'} -$$

$$-\tfrac{1}{3} \frac{\hat{J}_\alpha}{\hat{j}_{n'}} \sum_{a \le a'} H_{\rm hh}(aa'nn'J_\alpha) \left(v_a v_{a'} X^\alpha_{aa'} - u_a u_{a'} Y^\alpha_{aa'} \right) \sigma^{-1}_{aa'} +$$

$$+\tfrac{1}{3} \frac{\hat{J}_\alpha}{\hat{j}_{n'}} \sum_{a \le a'} H_{\rm ph}(aa'nn'J_\alpha) \left(u_a v_{a'} X^\alpha_{aa'} + v_a u_{a'} Y^\alpha_{aa'} \right) \sigma^{-1}_{aa'} \tag{15}$$

$$-\tfrac{1}{3} \frac{\hat{J}_\alpha}{\hat{j}_{n'}} \sum_{a \le a'} H_{\rm hp}(aa'nn'J_\alpha) \left(v_a u_{a'} X^\alpha_{aa'} + u_a v_{a'} Y^\alpha_{aa'} \right) \sigma^{-1}_{aa'} \,,$$

where

$$H_{\rm pp}(nn'aa'J) = 2v_n u_{n'} G(nn'aa'J) \,, \tag{16}$$

$$H_{\rm hh}(nn'aa'J) = 2u_n v_{n'} G(nn'aa'J) \,, \tag{17}$$

$$H_{\rm ph}(nn'aa'J) =$$

$$2v_n v_{n'} F(nn'aa'J) + 2u_n u_{n'} F(n'naa'J)(-1)^{j_n + j_{n'} + J} \,, \tag{18}$$

$$H_{\rm hp}(nn'aa'J) =$$

$$2u_n u_{n'} F(nn'aa'J) + 2v_n v_{n'} F(n'naa'J)(-1)^{j_n + j_{n'} + J} \,. \tag{19}$$

The overlap between the one-quasiparticle and the quasiparticle-phonon states is always zero. However, the overlap between two quasiparticle-phonon states can be non-zero and the quasiparticle-phonon states form a non-orthogonal over-complete basis set. The ansatz (12) leads to a generalized hermitian (or real and symmetric) eigenvalue problem which has the form [19] :

$$\sum_j H_{ij} C^{(n)}_j = \lambda_n \sum_j S_{ij} C^{(n)}_j \,. \tag{20}$$

where $H_{ij} = \langle i|H|j\rangle$ and $S_{ij} = \langle i|j\rangle$ is the overlap matrix element between two basis states (one-quasiparticle or quasiparticle-phonon states). To solve this rather involved eigenvalue problem we adopt the method where we first solve the eigenvalue equation for the overlap matrix $\mathbf{S}$:

$$\sum_j S_{ij} u^{(k)}_j = n_k u^{(k)}_i \,. \tag{21}$$

The eigenvectors of eq. (21) can be written in the basis $\{|i\rangle\}$ as

$$|\tilde{k}\rangle = \frac{1}{\sqrt{n_k}} \sum_i u_i^{(k)} |i\rangle \,. \tag{22}$$

They have the property of being mutually orthogonal, have a norm equal to unity and form a complete set after removing states having eigenvalue $n_k = 0$ (this removes the overcompleteness of the set $\{|i\rangle\}$). Using the new orthogonal complete set of states (22) we can transform (20) to an ordinary real and symmetric eigenvalue problem of the form:

$$\sum_j \langle\tilde{i}|H|\tilde{j}\rangle g_j^{(n)} = \lambda_n g_i^{(n)} \,, \tag{23}$$

where

$$\langle\tilde{i}|H|\tilde{j}\rangle = \frac{1}{\sqrt{n_i n_j}} \sum_{kl} u_k^{(i)*} \langle k|H|l\rangle u_l^{(j)} \,. \tag{24}$$

The coefficients of eigenstates are calculated from the g coefficients in the following way:

$$C_i^n = \sum_k n_k^{-1/2} g_k^{(n)} u_i^{(k)} \,. \tag{25}$$

In practical calculations one omits states (22) having eigenvalue n_k less than some set upper limit ϵ.

In the present work we have examined the β^+(EC) decay strength function of the ^{147}Tb $\rightarrow$ ^{147}Gd decay. To do this we have constructed the mother and daughter nuclei from ^{148}Dy and ^{148}Gd, respectively. This means that we have studied first the spectroscopy of the two aforementioned even-even nuclei to set the parameters of the interaction in a manner described earlier in the text. These nuclei then provide our quasiparticles and the QRPA phonons to be used in the ansatz of eq. (12). As the next step we construct ^{147}Tb as a proton-hole nucleus (^{148}Dy plus a proton quasiparticle) and ^{147}Gd as a neutron-hole nucleus (^{148}Gd plus a neutron quasiparticle). In this case the treatment of ^{147}Tb and ^{147}Gd as particle nuclei based on ^{146}Gd would not be reliable since ^{146}Gd has magic neutron number N=82 and the BCS treatment of closed shells is

not possible. Only further away from the magic numbers the particle and hole treatments are symmetric [19].

We have performed the calculations in the s-d-g and p-f-h oscillator major shells supplemented by the $i_{13/2}$ intruder orbital from the next oscillator major shell. We use the same valence space for neutrons and protons. In this case no adjustment of the single-particle energies was done but the mean-field part was taken directly from the Woods–Saxon calculation. The quadrupole part of the two-body interaction was fixed by fitting the experimental energy of the first 2^+ state in ^{148}Dy and ^{148}Gd nuclei. The other multipolarities were assumed to have their bare G-matrix value. In the diagonalization of the MQPM super matrix of eq. (20) we have used 4 lowest QRPA phonons of multipolarity 2^+, 3^-, 4^+, 5^- and 6^+. This number of selected multipolarities is enough to stabilize the spectrum of ^{147}Tb and ^{147}Gd.

4.2. Expressions for allowed beta decay

In the calculation of beta-decay transition amplitudes one has to know the matrix elements of the charge-changing transition densities (CCTD) between the initial and final states. The transition amplitude is expressed in terms of matrix elements of the CCTD and the single-particle matrix elements of the transition operator. In the following equations we write explicit expressions of all the needed reduced matrix elements.

In our formalism we employ the following reduced matrix elements of the CCTD between one-quasiparticle states

$$(-||a_n \left[c_{n'}^\dagger \tilde{c}_{p'}\right]_L a_p^\dagger||-) = \hat{L} u_n u_p \delta_{nn'} \delta_{pp'} \,, \tag{26}$$

$$(-||a_p \left[c_{n'}^\dagger \tilde{c}_{p'}\right]_L a_n^\dagger||-) = \hat{L} v_p v_n \delta_{pp'} \delta_{nn'} (-1)^{j_{p'}+j_{n'}+L} \,, \tag{27}$$

$$(-||a_p \left[c_{p'}^\dagger \tilde{c}_{n'}\right]_L a_n^\dagger||-) = \hat{L} u_p u_n \delta_{pp'} \delta_{nn'} \,, \tag{28}$$

$$(-||a_n \left[c_{p'}^\dagger \tilde{c}_{n'}\right]_L a_p^\dagger||-) = \hat{L} v_n v_p \delta_{nn'} \delta_{pp'} (-1)^{j_{n'}+j_{p'}+L} \,. \tag{29}$$

These equations describe β^+(EC) transitions between particle states, β^+(EC) transitions between hole states, β^- transitions between particle

states and β^- transitions between hole states, respectively. Reduced matrix elements of the CCTD between a quasiparticle-phonon state and a one-quasiparticle state are:

$$(-||\left[Q_\alpha a_n\right]_j \left[c^\dagger_{n'} \tilde{c}_{p'}\right]_L a^\dagger_p||-) = \hat{J}_\alpha \hat{L} \hat{j} \times$$

$$\left[\left\{ \begin{matrix} j_p & j & L \\ j_n & j_{p'} & J_\alpha \end{matrix} \right\} \bar{X}^\alpha_{pp'} u_{n'} v_{p'} \delta_{nn'} (-1)^{j_p+j+L} + \frac{\delta_{jj_{n'}}}{\hat{j}^2} \bar{Y}^\alpha_{nn'} v_{n'} u_{p'} \delta_{pp'} \right] , \quad (30)$$

$$(-||\left[Q_\alpha a_p\right]_j \left[c^\dagger_{n'} \tilde{c}_{p'}\right]_L a^\dagger_n||-) = -(-1)^{j_{n'}+j_{p'}+L} \times \hat{J}_\alpha \hat{L} \hat{j} \times$$

$$\left[\left\{ \begin{matrix} j_n & j & L \\ j_p & j_{n'} & J_\alpha \end{matrix} \right\} \bar{X}^\alpha_{nn'} v_{n'} u_{p'} \delta_{pp'} (-1)^{j_n+j+L} + \frac{\delta_{jj_{p'}}}{\hat{j}^2} \bar{Y}^\alpha_{pp'} u_{p'} v_{n'} \delta_{nn'} \right] . \quad (31)$$

In equations (30) and (31) only the matrix elements corresponding to eqs. (26) and (27) are shown. The other two are obtained by interchanging the proton and neutron indices. The reduced matrix elements of the CCTD between two quasiparticle-phonon states are:

$$(-||\left[Q_\alpha a_n\right]_j \left[c^\dagger_{n'} \tilde{c}_{p'}\right]_L \left[a^\dagger_p Q^\dagger_{\alpha'}\right]_{j'}||-) =$$

(32)

$$\hat{j} \hat{L} \hat{j}' \left\{ \begin{matrix} j' & j & L \\ j_{n'} & j_p & J_{\alpha'} \end{matrix} \right\} u_{n'} u_{p'} (-1)^{j+L+j'} \times$$

$$\left[\delta_{nn'} \delta_{pp'} \delta_{\alpha\alpha'} + \delta_{pp'} \hat{J}_\alpha \hat{J}_{\alpha'} \sum_a \left(\left\{ \begin{matrix} j & J_\alpha & j_n \\ j_a & J_{\alpha'} & j_{n'} \end{matrix} \right\} \bar{X}^\alpha_{n'a} \bar{X}^{\alpha'}_{na} - \frac{\delta_{jj_a}}{\hat{j}^2} \bar{Y}^\alpha_{na} \bar{Y}^{\alpha'}_{n'a} \right) \right]$$

$$+ \hat{j} \hat{L} \hat{j}' \left\{ \begin{matrix} j & j' & L \\ j_{p'} & j_n & J_\alpha \end{matrix} \right\} u_{n'} u_{p'} (-1)^{j+L+j'} \times$$

$$\left[\delta_{nn'} \delta_{pp'} \delta_{\alpha\alpha'} - \delta_{nn'} \hat{J}_\alpha \hat{J}_{\alpha'} \sum_a \left(\left\{ \begin{matrix} j' & J_{\alpha'} & j_p \\ j_a & J_\alpha & j_{p'} \end{matrix} \right\} \bar{X}^\alpha_{ap} \bar{X}^{\alpha'}_{ap'} - \frac{\delta_{j'j_a}}{\hat{j}'^2} \bar{Y}^\alpha_{ap'} \bar{Y}^{\alpha'}_{ap} \right) \right]$$

$$- \hat{j} \hat{L} \hat{j}' \hat{J}_\alpha \hat{J}_{\alpha'} v_{n'} v_{p'} \times$$

$$\left[\left\{ \begin{matrix} j & j' & L \\ J_\alpha & j_p & j_{p'} \\ j_n & J_{\alpha'} & j_{n'} \end{matrix} \right\} \bar{X}^\alpha_{pp'} \bar{X}^{\alpha'}_{n'n} (-1)^{j_{n'}+j_{p'}+L} + \frac{\delta_{jj_{n'}} \delta_{j'j_{p'}}}{\hat{j}^2 \hat{j}'^2} \bar{Y}^\alpha_{nn'} \bar{Y}^{\alpha'}_{p'p} \right] .$$

This matrix element again corresponds to equation (26). The other three matrix elements are obtained by interghanging the proton and neutron indices and/or making the substitution $u_a \rightarrow v_a$, $v_a \rightarrow -u_a$. The final

expressions for the Gamow-Teller transition amplitudes, for the comparative half-life ($\log(ft)$) and the expressions for the reduced single-particle matrix elements can be found e.g. in [15, 18]. After the calculations of the beta decay matrix elements one can calculate the beta decay strength function by using eqs. (1) and (2), or the $\log(ft)$ values. The beta decay strength function of (1) is proportional to $1/ft$.

5. Calculated results and comparison with experiment

Our theoretical results on the ^{147g}Tb $\rightarrow$ ^{147}Gd β^+(EC) decay have been summarized in Table 1 where we give only the final states with strongest beta feeding in the Q_{EC}-window and omit the rest. In this table we show the excitation energy of the final state with respect to the ground state of ^{147}Gd (first column), its spin and parity (second column) and, finally, the $\log(ft)$ value of the corresponding Gamow-Teller transition. The initial state is the ^{147g}Tb ground state which in our calculation has as a dominating component the structure ^{147g}Tb(g.s.) = ^{146}Gd $\otimes$ $\pi 2s_{1/2}$ corresponding to the experimentally observed $1/2^+$ ground state of ^{147g}Tb. The resulting theoretical half-life for ^{147g}Tb is 3.8h.

An interesting observation results from Table 1. At around 3.3 MeV and 4.4 MeV of excitation there are very strong Gamow-Teller feedings of final states. The state at 3.3 MeV is a $1/2^+$ state and the analysis of the wave function of this excitation shows that the dominating component in the ansatz (5) is the following: ^{147}Gd$(1/2^+) \approx$ ^{146}Gd$(3^-_1) \otimes \nu 1f_{7/2}$, i.e. the odd neutron particle on the $1f_{7/2}$ orbital has coupled to the very collective first 3^- phonon of ^{146}Gd. This phonon is predominantly made of proton degrees of freedom since the neutrons occupy a closed shell. Analysis of this phonon indicates that the leading single-particle transitions are of the type $\pi 2s_{1/2} \rightarrow \nu 2s_{1/2}$, i.e. the neutron part of the final-state 3^- phonon is broken, and of the type $\pi 1f_{7/2} \rightarrow \nu 1f_{7/2}$ and $\pi 1f_{5/2} \rightarrow \nu 1f_{7/2}$, where this contribution arises from the ^{146}Gd$(3^-_1) \otimes \pi 1f_{7/2}$ and ^{146}Gd$(3^-_1) \otimes \pi 1f_{5/2}$ components of the initial ground state.

At 4.4 MeV of excitation there are very strong transitions to a $1/2^+$ and $3/2^+$ state. Both of these states have as the dominating structure ^{146}Gd$(5^-_1) \otimes \nu 0h_{9/2}$, i.e. the odd neutron particle on the $0h_{9/2}$ orbital has coupled to the collective first 5^- phonon of ^{146}Gd. In this case the by far leading single-particle transition is of the type $\pi 0h_{11/2} \rightarrow \nu 0h_{9/2}$ arising from breaking the proton part of the 5^-_1 phonon of the final state.

Table 1: The Gamow-Teller β^+/EC decay of the ground state of ^{147g}Tb to excited states of ^{147}Gd. The first column the excitation energy (relative to $147Gd$ ground state) and the second the spin and parity of the final state. The third column gives the log(ft) value of the transition to this state.

Exc. energy	Spin	log(ft)
0.66	$1/2^+$	9.5
1.41	$3/2^+$	9.6
1.44	$1/2^+$	9.0
1.63	$1/2^+$	9.2
2.21	$1/2^+$	9.2
2.66	$1/2^+$	9.5
2.75	$3/2^+$	9.2
2.75	$1/2^+$	8.9
3.32	$3/2^+$	7.6
3.33	$1/2^+$	5.4
3.69	$1/2^+$	9.6
4.43	$1/2^+$	4.0
4.43	$3/2^+$	4.5

As described above, our calculation predicts at around 4 MeV a strong peak in $S_{(EC)}(E)$ corresponding to strong Gamow–Teller feeding of the $1/2^+$ and $3/2^+$ states in ^{147}Gd. This theoretical result is in qualitative agreement with the experiment. A strong peak with a width ≥ 0.5 MeV and $log(ft) \simeq 5.3$ is experimentally observed in $S_{(EC)}(E)$ in the region $E \simeq 4$ MeV (Fig. 5a and 5b). However, our calculation predicts far less intense peaks in $S_{\beta^+(EC)}(E)$ in the low-energy region than experimental ones and gives a good 2 times larger half-life of ^{147g}Tb. The reason for this might be the vicinity of the $N = 82$ shell closure which seems to reflect too strongly to the details of the calculated wave functions of ^{147}Tb and/or ^{147}Gd.

It should be mentioned that the currently developed theoretical approaches to description of the structure of the strength function for beta transitions [2, 4, 18, 20, 21] are able to provide correct qualitative trends

but do not always allow for a detailed description of $S_\beta(E)$. Especially theories which are based on the quasiparticle concept face troubles in the immediate vicinity of proton or neutron closed shells.

6. Conclusion

1. Using our total absorption spectrometer, one can get information on the structure of strength functions for beta transitions. In the excitation energy region $E \leq 5$ MeV, no nuclear decay scheme data are needed for gaining information on the structure of $S_\beta(E)$ provided that total absorption peaks are identified. If the range is $E \geq 5$ MeV or in the range where the total absorption peaks are not identified, the analysis of TAS-gamma-spectra is more difficult and requires information on details of the relevant nuclear decay schemes.

2. The strength function for the β^+(EC) decay of the ^{147g}Tb (1.6 h) has a distinct resonance character.

3. The currently used theoretical approaches to description of the strength function $S_{\beta^+(EC)}(E)$ usually provide only a correct qualitative picture of the β decay but do not ensure detailed description of the process for a wide range of nuclei.

References

1. Ikeda K. // Prog. Theor. Phys., 1964, V.31. P.434.
2. Naumov Yu.V., Bykov A.A., Izosimov I.N. // Sov. J. Part. Nucl., 1983. V.14(2). P.175 (Translated by American Institute of Physics).
3. Dshelepov B.S., Zirianova L.N., Suslov Yu.P. // Beta-decays, ed. by Science Press, Leningrad, 1972.
4. Moller P., Randrup J. // Nucl. Phys., 1990. V.A514. P.1
5. Izosimov I.N., Naumov Yu.V. // Izv. AN SSSR, ser.fiz., 1978. V.42. P.2248.
6. Klapdor H.V. // Fortschr.d.Phys., 1985. V.33. P.1.
7. Klapdor H.V. // Phys. Lett., 1976. V.65B. P.35.
8. Wene C.O., Klapdor H.V. // Proc. Int. Conf. on Nuclear Structure (Tokyo, 1977). P. 797.
9. Wawryszczuk J., Yuldashev M.B., Gromov K.Ya., Fominykh V.I., Sereeter Sh., Kalinnikov V.G., Kotovskij N.Yu., Kalyapkin K.V., Potempa A.W., Izosimov I.N., Myakushin M.Yu., Rimski-Korsakov A.A., Muminov T.M. // Preprint JINR, E6-95-514, Dubna, 1995.
10. Kalinnikov V.G. et al. // Nucl. Instruments and Methods, 1992. V.B70. P.62.
11. Izosimov I.N., Lazarev Yu.A., Myakushin M.Yu., Rimski-Korsakov A.A., Shirakovski I.V., Sobolev Yu.G., Subbotin V.G. // Heavy Ion Physics Scintific Report, FLNR, Dubna, 1991-1992, p.211.
12. Bykov A.A., Vitman V.D., Naumov Yu.V., Orlov S.Yu., Tarasov V.K. // Preprint LINP N 628, Leningrad, 1980.
13. Bykov A.A., Vitman V.D., Naumov Yu.V., Orlov S.Yu., Tarasov V.K. // Preprint LINP N 647, Leningrad, 1981.
14. Holinde K. // Phys. Reports, 1981. V. 68. P.121.
15. Suhonen J., Taigel T., Faessler A. // Nucl. Phys., 1988. V. A486. P. 91.
16. Bohr A., Mottelson B.R. // Nuclear Structure. V. 1 (Benjamin, New York, 1969).
17. Ring P., Schuck P. // The nuclear many-body problem (Springer, 1980).
18. Suhonen J. // Nucl. Phys., 1993. V. A563. P. 205.
19. Toivanen J., Suhonen J. // J. Phys., 1995. V. G21. P. 1491.

20. Gaponov Yu.V., Lutostanski Yu.S. // Sov. J. Part. Nucl., 1982. V.12. P.1324.
21. Guba V.G., Nikolaev M.A., Urin M.G. // Proc. of the LINP XXXIII Winter School. Leningrad. 1989.P.364.

Received by Publishing Department on December 5, 1996.